

Discovery of spin glass in maple-leaf lattice $\text{Na}_2\text{Mn}_3\text{O}_7$

Iwnetim I. Abate^{1,2,3,+,*}, Lilia S. Xie^{1,+}, Hari Ramachandran⁴, Shivani Srivastava^{2,5}, Mark Asta^{2,5}, Kwabena Bediako^{1,6*}

1. *Department of Chemistry, University of California, Berkeley, California 97420, USA*
2. *Department of Materials Science & Engineering, University of California, Berkeley, California 97420, USA*
3. *Current Address: Department of Materials Science and Engineering, Massachusetts Institute of Technology, Cambridge, MA 02139, USA*
4. *Department of Materials Science and Engineering, Stanford University, 496 Lomita Mall, Stanford, CA 94305, USA.*
5. *Materials Sciences Division, Lawrence Berkeley National Laboratory, Berkeley, CA 94720, USA*
6. *Chemical Sciences Division, Lawrence Berkeley National Laboratory, Berkeley, CA 94720, USA*

[*] *Corresponding-Author, E-mail: iabate@berkeley.edu, bediako@berkeley.edu*

[+] *These authors contributed equally to this work*

Abstract

Geometrically frustrated magnetism is commonly studied in triangular and Kagome lattices. A rare lattice which exhibits frustration is obtained by depleting 1/7 of the sites from a triangular lattice and is called a maple-leaf lattice. We report the magnetic properties of an oxide material with a maple-leaf lattice: $\text{Na}_2\text{Mn}_3\text{O}_7$. Structural studies suggest slight lattice distortion and density functional theory predicts energetic near-degeneracy between ferromagnetism and antiferromagnetic phases which points towards competing magnetic orderings at low temperatures. In addition, from our magnetic studies, we discovered a non-equilibrium spin state below ~50 K. The bifurcation of field-cooled and zero-field-cooled magnetization curves, hysteresis of ~16 kOe at 2 K, and time-dependent magnetization response is consistent with a spin glass state. To our knowledge this is the first report of such a state in materials with a MLL. This is a promising discovery towards using spin glass to transport angular momentum or spins for applications low power spintronics.

Introduction

Spin glasses, which harbor a multitude of ground-state degeneracies, have drawn considerable interest over the past few decades because they provide a platform to study non-equilibrium physics and can be used to transport angular momentum or spins for application in spintronics.¹ They are formed due to disorder and frustration. Quantifying and controlling the degree of disorder and frustration will enable the engineering of spin-glasses and to discover even new phases. Most of the studies in geometrically frustrated magnetism are on triangular and Kagome lattices. By depleting 1/7 of the sites (i.e. controlling the level depletion to engineer frustration and disorder) from a triangular lattice one can create the so called maple-leaf lattice (MLL). Depletion of 1/4 of sites from a triangular lattice leads to a Kagome lattice; therefore, the level of depletion (and perhaps level of disorder and frustration in MLL) sits right between triangular and Kagome.² An oxide material with a MLL is $\text{Na}_2\text{Mn}_3\text{O}_7$ ³⁻⁶, which possess ordered vacancies at one out of every potential seven Mn sites. These ordered vacancies result in geometric frustration due to their configuration in the MLL, which might be envisioned to produce distinctive physical phenomena, by analogy to the properties that emerge in other solids with geometrically frustrated structures, such as Kagome lattices. However, fundamental physical measurements of materials with the MLL structure remain limited due to the existence of only a few material candidates with such configurations compared to triangular or Kagome lattices. Furthermore, other known materials with MLL structures often contain nonmagnetic impurities or extra magnetic ions between the layers, which can obscure the intrinsic properties of the MLL.^{7,8} The manganese oxides $\text{Na}_2\text{Mn}_3\text{O}_7$ and $\text{MgMn}_3\text{O}_7 \cdot 3\text{H}_2\text{O}$ ⁹, which can be synthesized without impurities and extra magnetic ions between layers, are ideal platforms to study the magnetic properties of MLL materials.

Here, we seek to investigate the magnetic properties of $\text{Na}_2\text{Mn}_3\text{O}_7$ to elucidate whether the geometric frustration of the MLL leads to a spin glass state. Combining ac and dc magnetization measurements and DFT calculations, we find that, contrary to previous studies,⁵ while AFM interactions dominate at high temperature, the geometrically frustrated maple-leaf lattice and resulting structural variation in Mn coordination environments engenders a disordered non-equilibrium spin state below ~50

K. The observed low temperature behavior, which includes bifurcation of field-cooled and zero-field-cooled magnetization curves, hysteresis of ~ 16 kOe at 2 K, and time-dependent magnetization response, is consistent with a spin glass state. To our knowledge this is the first report of such a state in materials with MLL. DFT calculations suggest a minimal difference in energy between FM and AFM configuration. (near-degeneracy). Presence of multiple possible near-degenerate orders,¹⁰ in addition the distorted lattice, are sources of the observed frustrated magnetism and spin-glass.

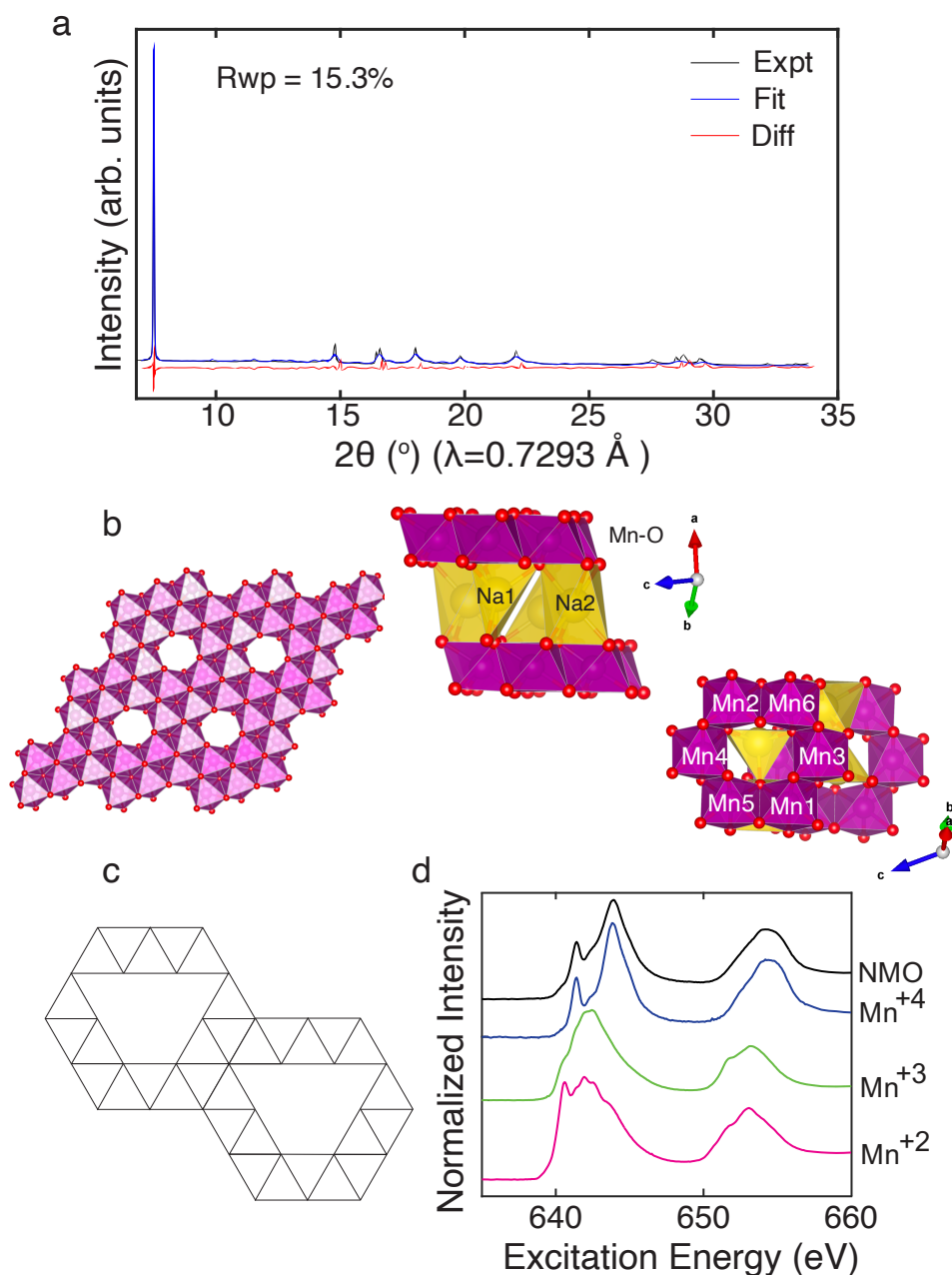


Figure 1 (a) Room-temperature X-ray diffraction pattern and Rietveld refinement for polycrystalline powder of $\text{Na}_2\text{Mn}_3\text{O}_7$. The parameters for the best-fit results obtained from the Rietveld refinement are also shown. (b) Schematic of top and side view of $\text{Na}_2\text{Mn}_3\text{O}_7$ crystal structure. The two-dimensional layered arrangement of MnO_6 polyhedral sheet is separated by the nonmagnetic Na (yellow) layer. The arrangement of magnetic Mn^{4+} (magenta) ion within the MnO_6 octahedra. The six unique Mn atoms in the MnO_6 polyhedra are labeled. (c) Maple-leaf lattice. (d) Mn-L edge TEY-XAS. The magenta, green and navy blue spectra are for reference compounds with Mn^{+2} (MnO), Mn^{+3} (Mn_3O_4), and Mn^{+4} ($\text{Li}_{1.17}\text{Ni}_{0.21}\text{Co}_{0.08}\text{Mn}_{0.54}\text{O}_2$).

Methods

$\text{Na}_2\text{Mn}_3\text{O}_7$ powder was prepared using a solid-state method. A stoichiometric mixture of NaNO_3 (J. T. Baker, A.C.S. Reagent) and MnCO_3 (Aldrich, $\geq 99.9\%$) powder was mixed with mortar and pestle for 30 mins. The collected mixture powder was then heated at 600°C ($5^\circ\text{C}/\text{min}$) for 12 h under oxygen flow. The prepared powder sample was left to cool down naturally to 150°C under oxygen flow before it was transferred directly to an argon-filled glovebox (MBraun, O_2 and $\text{H}_2\text{O} \leq 0.1$ ppm) without air exposure. High-resolution powder XRD (17 keV (0.7293 \AA) beam energy) and Mn-L edge XAS ($40 \times 40 \mu\text{m}$ slits, 1010 photons / sec and $1 \times 1 \text{ mm}^2$ spot size) were measured at beamline 2-1 and 8-2 at the Stanford Synchrotron Radiation Lightsource (SSRL, SLAC National Accelerator Laboratory), respectively. All magnetometry experiments were performed on a Quantum Design Physical Property Measurement System equipped with a 12 T magnet. Dc magnetization was measured using the Vibrating Sample Magnetometer option, whereas ac magnetometry was carried out using the AC Measurement System option. (An adapted cooling protocol was used to ensure the absence of negative trapped field.¹¹)

Computational studies were performed with density-functional theory (DFT). Specifically, lattice relaxation and total energy calculations were performed using the Projector-Augmented Wave (PAW) method,¹² as implemented in the Vienna Ab initio Simulation Package (VASP).¹³ Use was made of the spin-

polarized Perdew–Burke–Ernzerhof (PBE) generalized gradient approximation (GGA).^{12,14,15} with Hubbard U corrections (GGA+U), following the formalism of Dudarev¹⁶ with values of $U_{\text{eff}}=U-J=3.9$ eV for Mn d , and 4.5 eV for O p electrons.⁴ The PAW potentials employed in the calculations treated the following electronic states as valence: Na: $3s^1$, Mn: $4s^1$, $3p^6$, $3d^6$ and O: $2s^2$, $2p^4$. The Brillouin zone was sampled with a $4\times4\times4$ Monkhorst–Pack k-point grid, employing Gaussian smearing of 0.05 eV. The plane-wave cut-off was 600 eV. Relaxation of ions and cell shape was performed with convergence criteria of 10^{-5} eV in total energy, and until the forces on the atoms reached a magnitude less than 0.01 eV \AA^{-1} , respectively.

Results and Discussions

Rietveld refinement of the PXRD data revealed structural parameters for $\text{Na}_2\text{Mn}_3\text{O}_7$ consistent with previous literature reports and confirmed the absence of any phase impurities (confirmed by Energy-dispersive X-ray spectroscopy analysis; Na:Mn:O:C=16.38:45.70:29.68:8.25 wt%).⁶ Figure 1a shows the experimentally measured XRD pattern and the Rietveld refinement fitting profile. P1 crystallographic symmetry was identified with lattice parameters $a = 6.5539$ \AA , $b = 6.936$ \AA , $c = 7.5521$ \AA , $\alpha = 105.92^\circ$, $\beta = 106.25^\circ$, and $\gamma = 111.01^\circ$, and with Mn atoms occupying six unique positions (Figure 1(b)). $\text{Na}_2\text{Mn}_3\text{O}_7$ is composed of $[\text{Mn}_3\text{O}_7]^{2-}$ layers built up with edge-sharing MnO_6 octahedra.^{5,17} The Na ions occupy two different sites between the layers, labeled Na1 and Na2, with trigonal prismatic and distorted octahedral coordination, respectively (Figure 1(b)). In addition, compared to a perfect triangular Mn lattice, 1/7 of the Mn ions are missing in an ordered fashion, giving rise to the characteristic maple-leaf lattice geometry, Figure 1 (c). Based on X-ray absorption spectroscopy (total fluorescence yield, TFY), the Mn ions exist in the +4 valence state, Figure 1 (d), with varying Mn–Mn distances and Mn–O–Mn angles based on the Rietveld refinements (Table 1), indicating strong lattice distortion.⁵ The Mn–Mn interlayer distance is much larger than the in-plane Mn–Mn distance (~ 6.5 vs. 2.8 \AA), resulting in weak interlayer coupling in $\text{Na}_2\text{Mn}_3\text{O}_7$. As a result, the magnetic behavior is expected to be quasi two-dimensional in nature,² making NMO a promising platform for studying non-equilibrium dynamics in low-dimensional magnetism.

Table 1 The Mn–Mn bond distances and bond angles (Mn–O–Mn) extracted from the Rietveld refinement of Na₂Mn₃O₇ XRD pattern.

Mn pair	Mn–Mn distance (Å)	Mn–O–Mn angle (°)	Mn–O–Mn angle (°)
Mn1–Mn3	2.769	O7 – 98.7	-
Mn1–Mn5	2.437	O11 – 63.6	-
Mn3–Mn6	3.276	O9 – 136.13	O13 – 111.12
Mn4–Mn5	3.275	O14 – 125.15	O10 – 163.17
Mn2–Mn6	2.288	O8 – 70.5	O12 – 62.6
Mn2–Mn4	2.638	O6 – 80.7	-

Temperature- (1.8–300 K) and field-dependent (50–5000 Oe) dc magnetic magnetization measurements revealed an upturn in the magnetic moment below ~50 K in both zero-field-cooled (ZFC) and field-cooled (FC) curves (Figure 2). This behavior suggests a transition away from the paramagnetic behavior observed at higher temperatures. Notably, the ZFC and FC curves deviate appreciably from one another at lower temperatures. With decreasing temperature, the ZFC curves show a down-turn of the moment, whereas the FC curves exhibit continuously increasing moments. The location of the bifurcation between ZFC and FC curves decreases monotonically with increasing fields from ~47 K at 50 Oe to ~20 K at 5000 Oe. Such behavior is a hallmark of disordered spin systems, including spin glasses.^{18,19}

The magnetic behavior of $\text{Na}_2\text{Mn}_3\text{O}_7$ at higher temperatures (250 K – 300 K) is characterized by a Curie–Weiss temperature, θ_{CW} , of –216 K and a Curie constant, C , of 6.15 emu K Oe^{–1} mol^{–1} (Figure 3). The negative value and appreciable magnitude of θ_{CW} is consistent with a prevalence of antiferromagnetic interactions in this temperature regime, possibly resulting from Mn–Mn direct exchange interactions.³ In addition, due to the distorted octahedral geometry around each Mn center, the Mn–O–Mn bond angles deviate considerably from 90° (Table 1). As a result, according to Goodenough–Kanamori rules, ferromagnetic Mn–O–Mn superexchange interactions are not expected, but antiferromagnetic superexchange interactions are possible.^{20,21} The value of the C is somewhat higher than the theoretical value of 5.63 emu K Oe^{–1} mol^{–1} for three Mn⁴⁺ ions (assuming $g = 2$ and $S = 3/2$). Overall, deviation from ideal Curie–Weiss behavior suggests that short-range interactions may affect the magnetization significantly, even up to 300 K. Additionally, the monotonically increasing value of $\chi_M T$ up to 300 K (Figure 3 inset) suggests that a temperature-independent term may also contribute to the observed moment at high temperatures. The somewhat different θ_{CW} and C compared to previous reports (–192 and –152 K for θ_{CW} ; 5.77 and 5.7 emu K Oe^{–1} mol^{–1} for C)^{3,5} may be due to slight differences in the composition or homogeneity of the samples, which could be dependent on the exact sample preparation procedure.

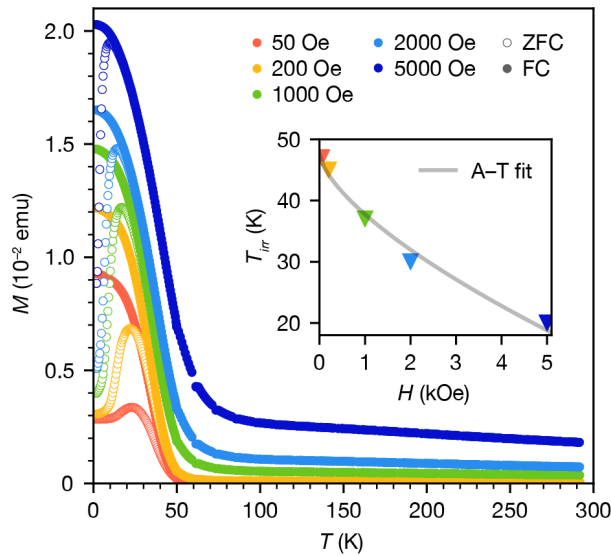


Figure 2. Temperature-dependent zero field-cooled (ZFC) and field-cooled (FC) dc magnetization under applied magnetic fields ranging from 50 to 5000 Oe. The ZFC and FC data at a given field are represented by open and closed symbols, respectively. Inset: The bifurcation temperatures of ZFC and FC data for different applied fields (solid triangles), fit to the de Almeida–Thouless relation (gray line).

The field dependence of the irreversible temperature suggests the presence of a metastable state with frozen spins exhibiting short-range order below the bifurcation temperature.²² To investigate the nature of this state, we extracted the irreversible temperatures (T_{irr}) from the bifurcation of ZFC and FC curves at each applied field and fit T_{irr} as a function of the applied magnetic field to the de Almeida–Thouless relation for spin glasses²³:

$$T_{irr}(H) = T_{irr}(0)(1 - RH^n)$$

where $T_{irr}(0)$ is the limit of the irreversible temperature at zero field (H) and theoretically corresponds to the spin glass freezing temperature T_f , R is a constant, and n is 2/3 for an ideal spin glass system (Figure 2 inset). Taking $n = 2/3$, we obtain a satisfactory fit, with $T_{irr}(0) = 48$ K. These results are consistent with a spin glass state in $\text{Na}_2\text{Mn}_3\text{O}_7$ below 48 K. The geometrically frustrated maple leaf lattice and lattice disorder (due to unequal Mn–Mn distances and Mn–O–Mn angles) are ingredients for spin glass freezing. The frustration protects the ergodicity of the system until it reaches the spin glass transition where a metastable phase is formed. In addition, our DFT calculation suggests that the energy difference between AFM and FM is only 2.75 meV/f.u. (10 times less than $k_B T$ at room temperature). This rather small energy difference indicates a near-degeneracy in ferromagnetic and antiferromagnetic order and as reported in previous studies can be a signature of competing super-exchange and direct exchange interactions in the maple leaf lattice.^{5,9} Since we do not expect this material to show itinerant magnetism due to localized Mn moments, the total energy method for calculating exchange constants should give reasonable results.^{24,25} As a very crude approximation, the difference in energy of FM and AFM configurations divided by the number of

nearest neighbors at each site should provide us an estimate of exchange constants. In this paper, we have not aimed at computing quantitative values for these exchange constants which will require sampling multiple magnetic configurations and larger supercells. Presence of multiple possible near-degenerate competing ordering of moments which can not all be satisfied simultaneously have previously been shown to lead towards the spin glass behavior, and we anticipate a similar origin of spin-glass state in this system.²⁶

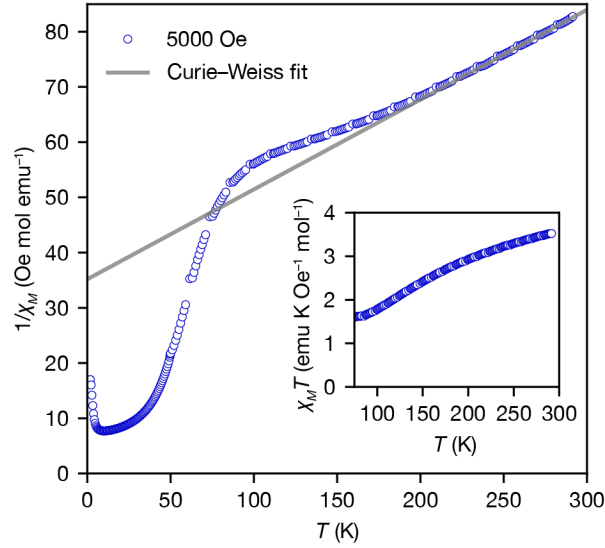


Figure 3 Inverse susceptibility vs. temperature data with a 5000 Oe field, fitted to the Curie–Weiss law between 250 and 300 K. Inset: $\chi_M T$ vs. temperature above the spin glass freezing temperature.

A unique signature of spin glass behavior is a frequency dependence to the real part (χ') of the ac magnetic susceptibility. To investigate the existence of the spin glass state further, we performed temperature-dependent ac susceptibility at frequencies (ν) between 27 and 9984 Hz with an applied ac magnetic field of 15 Oe (in no dc field). Figure 3a shows χ' in the vicinity of the putative spin glass transition. Indeed, a frequency-dependent cusp in χ' is observed around 35 K, where the temperature of the maximum (the freezing temperature, T_f) increases and peak height decreases with increasing frequency, providing additional evidence for a spin glass state in the MLL material Na₂Mn₃O₇.

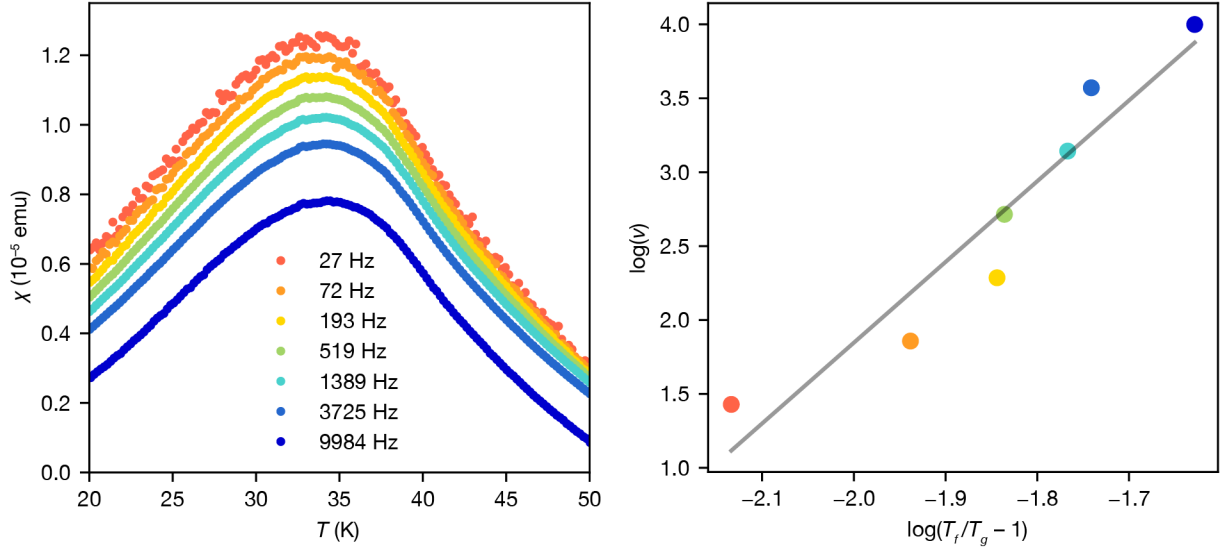


Figure 4. ac magnetic susceptibility. (a) Variation of the real part of the ac moment measured at different frequencies with temperature. (b) Fitting of the frequency-dependent freezing temperature with the power law, $\log(\nu)$ vs. $\log(T_f/T_g - 1)$.

A spin glass has a certain level of rigidity where upon application of an excitation wave, the spins respond together in a collective mode with correlation length ζ .²⁷ The rigidity of the spin glass can be quantified by calculating the Mydosh parameter (S), which measures the relative temperature shift per decade (sensitivity of the spin interactions to the applied excitation wave), as follows:

$$S = \frac{\Delta T_f}{T_f \Delta \log(\nu)}$$

where typical values of S for a spin glass lie between 0.005 and 0.08. Using the values from 27 and 9984 Hz, we calculated S to be 0.006 for $\text{Na}_2\text{Mn}_3\text{O}_7$, which is within the range for a canonical spin glass.^{28,29} The frequency-dependence of T_f can be described by slowing down of the spin-dynamics according to the critical scaling approach, which is described by:

$$\tau = \tau_0 \left(\frac{T_f}{T_g} - 1 \right)^{-z\nu'}$$

in which $\tau \sim \zeta^z$, where the correlation length $\zeta = \left(\frac{T_f}{T_g} - 1\right)^{-\nu'}$, T_g is the spin glass transition temperature, z is the freezing temperature in the limit $\nu \rightarrow 0$, and τ_0 is the relaxation time for a single spin flip. The best fitting of $\log_{10} \nu$ vs. $\log_{10}(T_f/T_g - 1)$ (Figure 4b) results in $z\nu' = 5.5(2)$ and $\tau_0 = 1 \times 10^{-12}$ s. The $z\nu'$ value falls in the range from 4–12 observed empirically for glassy systems and τ_0 is in the range for canonical spin glasses.^{10,30,31}

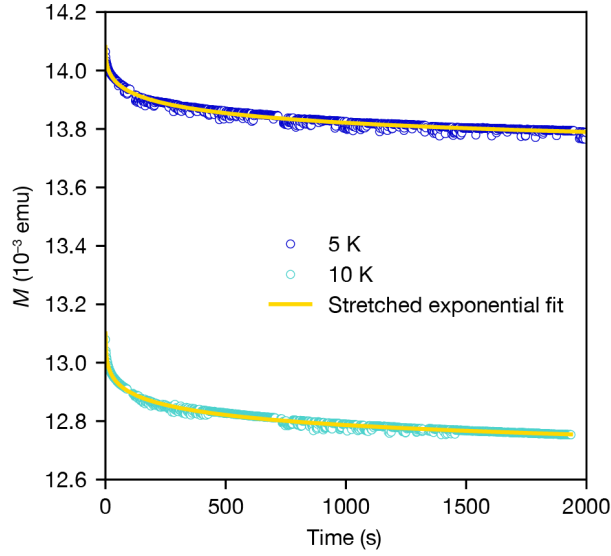


Figure 5. Thermoremanent magnetization (TRM) measurements were performed at 5 and 10 K after the samples were field-cooled in a field of 1000 Oe. The relaxations were measured after the magnetic field was removed.

We further probed the spin glass dynamics by performing time-dependent thermoremanent magnetization (TRM) experiments. We first cooled to either 5 K or 10 K in an applied field of 1000 Oe. Once the temperature was reached, we continued to apply the field for another 600 s before turning it off. The relaxation was then recorded for > 30 minutes, during which the slow decay of the isothermal remanent magnetization was observed, which is a characteristic of spin glass behavior (Figure 5). We fit the TRM data with a modified stretched exponential function:

$$M(t) = M_0 + M_g \exp \left[\left(-\frac{t}{\tau} \right)^{(1-n)} \right]$$

where M_0 and M_g are the intrinsic and glassy components of the moment, respectively, τ is the average relaxation time, and n is the time stretch exponent. The values of τ obtained for $\text{Na}_2\text{Mn}_3\text{O}_7$ are around 500 seconds at both 5 K and 10 K (Table 2), which are reasonable for a spin glass and indicate a clear evolution of the magnetization over time. The values of n , 0.67(1) and 0.73(1) at 5 K and 10 K, respectively, are also typical for spin glass systems.³²

Table 2. Parameters from fitting the time-dependent remanent magnetization to a modified stretched exponential function.

T (K)	M_0 (emu)	M_g (emu)	τ (s)	n
5	0.01371(1)	-0.00039(2)	530(50)	0.67(1)
10	0.01232(1)	-0.00052(2)	500(60)	0.73(1)

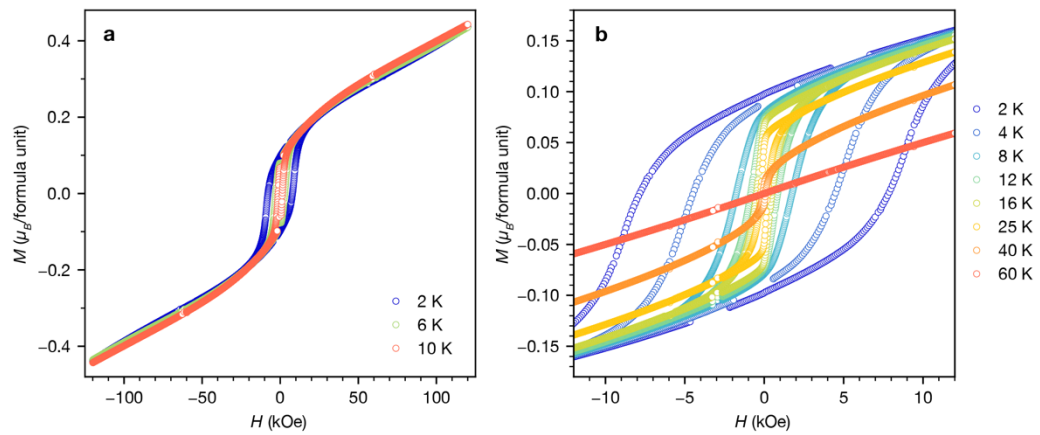


Figure 6 (a) Field-dependent dc magnetization measured at various temperatures between -120 and 120 kOe. (b) Enlarged view of hysteresis in field-dependent dc magnetization measured at various temperatures between -12 and 12 kOe.

Isothermal magnetization experiments revealed a lack of saturation in the magnetization values even at the largest applied fields of ± 120 kOe (Figure 6a). The maximum magnetization of $0.44 \mu_B/\text{formula unit}$ at $+12$ kOe is significantly less than expected for three Mn^{4+} ions in the paramagnetic regime ($6.70 \mu_B$), consistent with spin frustration from the maple leaf lattice. Notably, the curves exhibit pronounced hysteresis at temperatures lower than 40 K (Figure 6), with a hysteresis of about 16 kOe at 2 K. The hysteresis decreases with increasing temperature, narrowing to 200 Oe at 40 K and disappearing completely at 60 K to yield a linear magnetization vs. field response. This behavior is consistent with a spin glass state present at 40 K and below. Furthermore, the hysteresis indicates that an antiferromagnetically ordered ground state is not responsible for the magnetization behavior observed.

Field-cooling in ± 120 kOe fields at 2 K resulted in a small shift of the hysteresis curve along the field axis, consistent with the presence of a small intrinsic exchange bias (EB).^{33,34} The magnitude of the exchange bias is calculated as:

$$H_{EB} = (H_{C-} + H_{C+})/2$$

where $H_{C\pm}$ is the field at which the magnetization changes sign along an $M(H)$ curve. Figure 7a shows the low-temperature hysteresis loop (at 2 K) for samples cooled in -120 kOe and $+120$ kOe fields. The center of the hysteresis loop for the -120 kOe field-cooled trace shifts about $+40$ Oe, whereas the center of the $+120$ kOe field-cooled trace shifts about -30 Oe (Figure 8b and c), yielding an average EB of approximately -18 Oe. This very modest intrinsic EB may point to the existence of a small amount of uncompensated moments within the sample, or slight magnetic phase inhomogeneities.³⁵

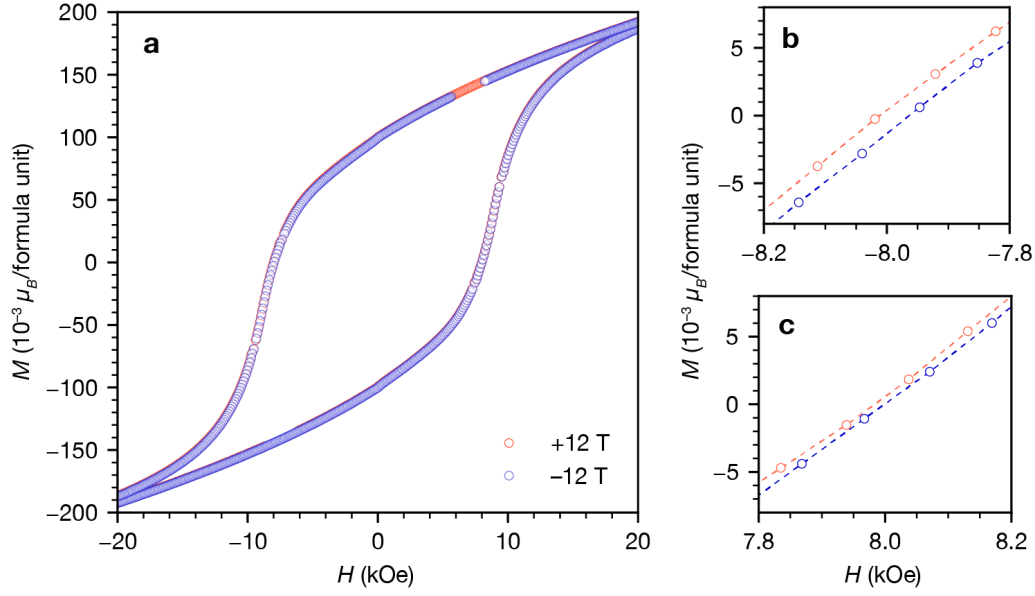


Figure 7. Exchange bias effect. (a) Isothermal magnetization curves after field-cooling in +120 kOe and – 120 kOe fields at 2 K. (b and c) Enlarged views of where the field-cooled magnetization curves change sign at both negative and positive fields, respectively.

Conclusion

We reported the first observation of a spin glass state in materials with a MLL configuration. By combining DFT with structural, spectroscopic, and magnetic characterization, we found that there is a near-degeneracy between FM and AFM configuration in $\text{Na}_2\text{Mn}_3\text{O}_7$, which coupled with the slightly distorted lattice, can explain frustrated magnetism that harbors spin glass behavior. Because $\text{Na}_2\text{Mn}_3\text{O}_7$ is one of the few MLL oxide materials without phase impurities, it is an ideal platform to study frustrated magnetism and spin glass dynamics in this structure. Modulation of magnetic properties may also be possible via de/intercalation of Na ions chemically or electrochemically. Since the MLL in $\text{Na}_2\text{Mn}_3\text{O}_7$ is formed by depleting 1/7 of Mn atoms from perfect triangular lattice, varying the amount of depletion could also present a future avenue to tune the strength and type of magnetic interactions. Advanced spectroscopy such as

resonant inelastic X-ray scattering could also shed light on the collective excitations that may exist in the spin glass. In addition, similar to the recent reports where a spin glass was used to transport angular momentum or spins in intercalated sulfides for applications in spintronics,¹ Na₂Mn₃O₇ could serve as a model system for an analogous phenomena in oxides.

Author Contributions

I. I. A. conceived the project; I. I. A. and K. B. supervised the experiments; I. I. A. and M. A. supervised the theoretical calculations; I. I. A. and H. R. synthesized the material. I. I. A. performed XAS; H. R. performed XRD; I. I. A. and L. S. X. performed the magnetization measurements and analysis. I. I. A. and S. S. performed the DFT calculations. I. I. A. and L. S. X. wrote the manuscript with inputs from all authors, I. I. A. and K. B. directed the overall research.

Conflicts of interest

No conflict of interest to declare.

Acknowledgments

The authors acknowledge Zhizhi Kong, Das Pemmaraju and Zhelong Jiang for insightful discussions. This material is based upon work supported by the Air Force Office of Scientific Research under AFOSR Award no. FA9550-20-1-0007. The authors also acknowledge the William Chueh Lab where some of synthesis and structural studies are performed. I.I.A acknowledges support from the Miller Institute for Basic Research in Science and Presidential Postdoctoral Fellowship at University of California, Berkeley. L.S.X. acknowledges support from the Arnold and Mabel Beckman Foundation (Award No. 51532) and L'Oréal USA (Award No. 52025) for postdoctoral fellowships. H.R. acknowledges funding support from the Knight-Hennessy Scholarship at Stanford University. S.S and M.A acknowledge funding support from the U.S. Department of Energy, Office of Science, Office of Basic Energy Sciences, Materials Sciences and Engineering Division, under Contract No. DE-AC02-05-CH11231 (Materials Project program

KC23MP). Instrumentation used in this work was supported by grants from the W.M. Keck Foundation (Award # 993922), the Canadian Institute for Advanced Research (CIFAR–Azrieli Global Scholar, Award # GS21-011), the Gordon and Betty Moore Foundation EPiQS Initiative (Award #10637), and the 3M Foundation through the 3M Non-Tenured Faculty Award (#67507585). The DFT calculations used computational resources from Extreme Science and Engineering Discovery Environment (XSEDE), which is supported by the National Science Foundation under Grant No. ACI-1548562.

Notes and references

- 1 E. Maniv, N. L. Nair, S. C. Haley, S. Doyle, C. John, S. Cabrini, A. Maniv, S. K. Ramakrishna, Y.-L. Tang, P. Ercius, R. Ramesh, Y. Tserkovnyak, A. P. Reyes and J. G. Analytis, *Sci. Adv.*, 2021, **7**, eabd8452.
- 2 R. Makuta and C. Hotta, *Phys. Rev. B.*, , DOI:10.1103/physrevb.104.224415.
- 3 A. Tsuchimoto, X.-M. Shi, K. Kawai, B. Mortemard de Boisse, J. Kikkawa, D. Asakura, M. Okubo and A. Yamada, *Nat. Commun.*, 2021, **12**, 631.
- 4 I. I. Abate, C. D. Pemmaraju, S. Y. Kim, K. H. Hsu, S. Sainio, B. Moritz, J. Vinson, M. F. Toney, W. Yang, W. E. Gent, T. P. Devereaux, L. F. Nazar and W. C. Chueh, *Energy Environ. Sci.*, , DOI:10.1039/d1ee01037a.
- 5 C. Venkatesh, B. Bandyopadhyay, A. Midya, K. Mahalingam, V. Ganesan and P. Mandal, *Phys. Rev. B.*, , DOI:10.1103/physrevb.101.184429.
- 6 B. Song, M. Tang, E. Hu, O. J. Borkiewicz, K. M. Wiaderek, Y. Zhang, N. D. Phillip, X. Liu, Z. Shadike, C. Li, L. Song, Y.-Y. Hu, M. Chi, G. M. Veith, X.-Q. Yang, J. Liu, J. Nanda, K. Page and A. Huq, *Chem. Mater.*, 2019, **31**, 3756–3765.
- 7 T. Fennell, J. O. Piatek, R. A. Stephenson, G. Nilsen and H. M. Ronnow, *arXiv [cond-mat.str-el]*, 2011.

- 8 A. Aliev, M. Huvé, S. Colis, M. Colmont, A. Dinia and O. Mentré, *Angew. Chem. Int. Ed Engl.*, 2012, **51**, 9393–9397.
- 9 Y. Haraguchi, A. Matsuo, K. Kindo and Z. Hiroi, *Phys. Rev. B.*, , DOI:10.1103/physrevb.98.064412.
- 10 J. A. Mydosh, *Spin glasses*, CRC Press, London, England, 1st Edition., 2014.
- 11 N. Kumar and A. Sundaresan, *Solid State Commun.*, 2010, **150**, 1162–1164.
- 12 P. E. Blöchl, *Phys. Rev. B Condens. Matter*, 1994, **50**, 17953–17979.
- 13 G. Kresse and J. Furthmüller, *Phys. Rev. B Condens. Matter*, 1996, **54**, 11169–11186.
- 14 J. P. Perdew, K. Burke and M. Ernzerhof, *Phys. Rev. Lett.*, 1998, **80**, 891–891.
- 15 G. Kresse and D. Joubert, *Phys. Rev. B Condens. Matter*, 1999, **59**, 1758–1775.
- 16 S. L. Dudarev, G. A. Botton, S. Y. Savrasov, C. J. Humphreys and A. P. Sutton, *Phys. Rev. B Condens. Matter*, 1998, **57**, 1505–1509.
- 17 B. Mortemard de Boisse, S.-I. Nishimura, E. Watanabe, L. Lander, A. Tsuchimoto, J. Kikkawa, E. Kobayashi, D. Asakura, M. Okubo and A. Yamada, *Adv. Energy Mater.*, 2018, **8**, 1800409.
- 18 N. A. Spaldin, in *Magnetic Materials*, Cambridge University Press, Cambridge, 2010, pp. 14–21.
- 19 R. Kumar, P. Yanda and A. Sundaresan, *Phys. Rev. B.*, , DOI:10.1103/physrevb.103.214427.
- 20 J. Kanamori, *J. Phys. Chem. Solids*, 1959, **10**, 87–98.
- 21 P. W. Anderson, *Phys. Rev.*, 1950, **79**, 350–356.
- 22 K. Binder and A. P. Young, *Rev. Mod. Phys.*, 1986, **58**, 801–976.
- 23 J. R. L. de Almeida and D. J. Thouless, *J. Phys. A Math. Gen.*, 1978, **11**, 983–990.
- 24 T. Moriya and Y. Takahashi, *J. Phys., Colloq.*, 1978, **39**, C6-1466-C6-1471.
- 25 X. Zhu, A. Edström and C. Ederer, *Phys. Rev. B.*, , DOI:10.1103/physrevb.101.064401.
- 26 L. Balents, *Nature*, 2010, **464**, 199–208.
- 27 B. I. Halperin and W. M. Saslow, *Phys. rev.*, 1977, **16**, 2154–2162.
- 28 D. X. Li, S. Nimori, Y. Shiokawa, A. Tobo, H. Onodera, Y. Haga, E. Yamamoto and Y. Ōnuki, *Appl. Phys. Lett.*, 2001, **79**, 4183–4185.

- 29 R. S. Freitas, L. Ghivelder, F. Damay, F. Dias and L. F. Cohen, *Phys. Rev. B Condens. Matter*, , DOI:10.1103/physrevb.64.144404.
- 30 A. Malinowski, V. L. Bezusyy, R. Minikayev, P. Dziawa, Y. Syryanny and M. Sawicki, *Phys. Rev. B Condens. Matter Mater. Phys.*, , DOI:10.1103/physrevb.84.024409.
- 31 J. Lago, S. J. Blundell, A. Eguia, M. Jansen and T. Rojo, *Phys. Rev. B Condens. Matter Mater. Phys.*, , DOI:10.1103/physrevb.86.064412.
- 32 P. Nordblad, P. Svedlindh, L. Lundgren and L. Sandlund, *Phys. Rev. B Condens. Matter*, 1986, **33**, 645–648.
- 33 M. Ali, P. Adie, C. H. Marrows, D. Greig, B. J. Hickey and R. L. Stamps, *Nat. Mater.*, 2007, **6**, 70–75.
- 34 W. H. Meiklejohn and C. P. Bean, *Phys. Rev.*, 1957, **105**, 904–913.
- 35 S. Karmakar, S. Taran, E. Bose, B. K. Chaudhuri, C. P. Sun, C. L. Huang and H. D. Yang, *Phys. Rev. B Condens. Matter Mater. Phys.*, , DOI:10.1103/physrevb.77.144409.